OPTICS, IMAGE SCIENCE, AND VISION

Terahertz time-domain ellipsometry: tutorial

ZAHRA MAZAHERI,[1] CAN KORAL,[1] ANTONELLO ANDREONE,[1,2,3,*] AND ANTIGONE MARINO[2,4]

[1]Physics Department, University of Naples Federico II, Naples, I-80126, Italy
[2]INFN, Naples Unit, Naples, I-80126, Italy
[3]Institute SPIN, CNR, Naples, I-80126, Italy
[4]CNR-ISASI, c/o University of Naples Federico II, Physics Department, Naples, I-80126, Italy
*Corresponding author: andreone@unina.it

Received 17 May 2022; revised 25 June 2022; accepted 28 June 2022; posted 30 June 2022; published 19 July 2022

Ellipsometry is extensively used in the optical regime to investigate the properties of many materials as well as to evaluate with high precision the surface roughness and thickness of thin films and multilayered systems. Due to the inherent *non-coherent* detection technique, data analyses in optical ellipsometry tend to be complicated and require the use of a predetermined model, therefore indirectly linking the sample properties to the measured ellipsometric parameters. The aim of this tutorial is to provide an overview of terahertz (THz) time-domain ellipsometry, which is based instead on a *coherent* detection approach and allows in a simple and direct way the measurement of the material response. After giving a brief description of the technology presently used to generate and detect THz radiation, we introduce the general features of an ellipsometric setup operating in the time domain, putting in evidence similarities and differences with respect to the classical optical counterpart. To back up and validate the study, results of THz ellipsometric measurements carried out on selected samples are presented. © 2022 Optica Publishing Group

https://doi.org/10.1364/JOSAA.463969

1. INTRODUCTION

Ellipsometry is a powerful, fast, reference-free, non-invasive technique for the characterization of materials. In the optical regime, it measures the intensity of the light beam reflected from the sample surface, inherently allowing *non-coherent* detection only. Time-domain techniques recently developed in the THz region make possible instead ellipsometry based on a *coherent* detection approach that provides in a simple and direct way the measurement of the material response. In this tutorial, we intend to present an overview of the emerging field of THz time-domain ellipsometry, putting in evidence similarities and differences with respect to the classical optical counterpart. After giving a historical introduction to the well-established optical ellipsometry, in Section 2, we shortly present—in a simplified manner—its constitutive relations. In Section 3, we introduce first a brief description on the technology presently used to generate and detect THz radiation and then the general features of an ellipsometric setup working in this frequency range. In Section 4, we illustrate the main equations governing the extraction of the material properties. Section 5 discusses calibration and setup issues affecting measurement sensitivity and accuracy. Section 6 is devoted to selected measurements carried out on some common solids and liquids to back up and validate the study. In the end, we draw some concise conclusions in Section 7.

In 1889, Drude first proposed the use of polarization to investigate the properties of matter and carried out ellipsometric measurements using the phase difference between two mutually perpendicular polarized light beams [1,2]. Rothen in 1945 introduced the name ellipsometry [3] in an experiment where the detector was simply the human eye. In his work published in 1962 in the *Journal of the Optical Society of America*, Archer proposed for the first time the possibility of integrating ellipsometry into industrial processes [4]. The leap in quality of the technique took place in the 1990s, when ellipsometry became spectroscopic, and spread to several laboratories and research centers. After a number of technological developments during the last years, we can safely say that ellipsometry is presently the mother technique for the optical study of thin films.

Ellipsometry arises from reflectometry; however, it is useful to understand the differences and similarities between these two techniques. They represent the reference methods for measuring samples consisting of a single or multilayer on a substrate. Single wavelength ellipsometry (SWE) can evaluate very thin layers, having thickness of a few Å or less. For thicker samples, reflectometry is faster. They both suffer if there is a lack of information on the nature of the materials under test or if there are too many layers to be measured. A major transformation occurred when technology helped scientists to develop spectroscopic ellipsometry (SE), a new technique that allows to analyze with ease

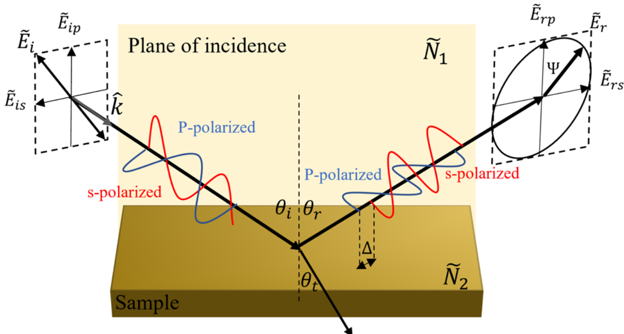

Fig. 1. Sketch of a linearly polarized light incident on and reflected from the flat surface of a sample having a complex refractive index $\tilde{N}_2$.

multilayered samples and determine the optical constant dispersion relationship of the constituent materials. SE is therefore an evolution of reflectometry, as it allows to measure many additional parameters of the investigated system, such as thickness [5], porosity, or concentration [6]. Generalized ellipsometry (GE) allows also to measure the anisotropy of materials [7–9].

The name ellipsometry arises from the most general form of light polarization, which is elliptical. Polarization ellipticity changes when light is reflected at an interface depending on the material optical constants and layer thickness. By measuring the reflection-induced ellipticity, it is possible to calculate the film properties. Figure 1 illustrates the case when a perfectly linear polarized light interacts with a material surface. A change in amplitude between s-polarized (polarization component perpendicular to the plane of incidence) and p-polarized (polarization component parallel to the plane of incidence) components takes place, as well as a relative phase delay, and upon reflection, the beam polarization state becomes elliptical. The plane of incidence is defined as the plane formed by the direction of propagation of the incident field and the axis orthogonal to the sample surface. θ_i is the angle of incidence, which in the case of a homogeneous material with a flat surface is equal to the angle of reflection θ_r. θ_t instead is the angle of beam transmission. In the following, we will assume $\theta_i = \theta_r = \theta$.

The measured value in ellipsometry is the complex ratio of the altered p-polarized $\tilde{E}_{rp}$ and s-polarized $\tilde{E}_{rs}$ components of the beam after interaction with a sample having complex refractive index $\tilde{N}_2 = n_2 - ik_2$, in comparison with their counterparts before reflection ($\tilde{E}_{ip}$ and $\tilde{E}_{is}$). n_2 and k_2 represent the refractive index and extinction coefficient of the sample, respectively. In the following, we will always assume $\tilde{N}_1 = 1$ (air).

The change appears in both the amplitude ratio and phase difference between p- and s-polarized reflected components. The quantity Ψ is defined as the angle whose tangent is the ratio between the modules of total reflection coefficients $\tilde{R}_p$ and $\tilde{R}_s$ of p and s waves, respectively, so that

$$\tan\Psi = \frac{|\tilde{R}_p|}{|\tilde{R}_s|} = \frac{|\tilde{E}_{rp}|/|\tilde{E}_{ip}|}{|\tilde{E}_{rs}|/|\tilde{E}_{is}|}. \tag{1}$$

The phase difference Δ instead is defined as

$$\Delta = \phi_p - \phi_s, \tag{2}$$

ϕ_p and ϕ_s being the phase of p- and s-polarized components after reflection, respectively. Positive (negative) values of Δ correspond to the left-handed (right-handed) elliptical polarization state of the beam. Ψ and Δ are called the ellipsometric angles and represent quantities describing the material optical properties. They can be summarized introducing the parameter $\rho \in \mathbb{C}$:

$$\rho \equiv \frac{\tilde{R}_p}{\tilde{R}_s} = \frac{|\tilde{R}_p|}{|\tilde{R}_s|}\frac{e^{i\phi_p}}{e^{i\phi_s}} = \tan\Psi e^{i\Delta}, \tag{3}$$

corresponding to the ratio of the (complex) reflection coefficients. ρ contains all the information on the response at the sample interface. Equation (3) is known as the fundamental equation of ellipsometry.

2. FUNDAMENTALS

To introduce the constitutive relations on which ellipsometry is based, we will define the polarization state of an electromagnetic wave and analyze the behavior at the interface between two materials in the most general case through the Fresnel coefficients.

Let us consider a plane interface between two isotropic dielectric materials with different refractive indices (Fig. 1). The electric field can be expressed as the sum of $\vec{E}_p$ and $\vec{E}_s$. Let us indicate with $\vec{E}_i$ the incident field and with $\vec{E}_r$ the reflected field, so that

$$\vec{E}_i = \vec{E}_{is} + \vec{E}_{ip},$$
$$\vec{E}_r = \vec{E}_{rs} + \vec{E}_{rp}. \tag{4}$$

Using the boundary conditions to connect the incident, reflected, and transmitted fields, it is possible to obtain expressions of the Fresnel coefficients

$$\tilde{R}_p \equiv \frac{\tilde{E}_{rp}}{\tilde{E}_{ip}} = \frac{\tilde{N}_1\cos\tilde{\theta}_t - \tilde{N}_2\cos\theta}{\tilde{N}_1\cos\tilde{\theta}_t + \tilde{N}_2\cos\theta} = \frac{\tan(\tilde{\theta}_t - \theta)}{\tan(\tilde{\theta}_t + \theta)}, \tag{5}$$

$$\tilde{R}_s \equiv \frac{\tilde{E}_{rs}}{\tilde{E}_{is}} = \frac{\tilde{N}_1\cos\theta - \tilde{N}_2\cos\tilde{\theta}_t}{\tilde{N}_1\cos\theta + \tilde{N}_2\cos\tilde{\theta}_t} = \frac{\sin(\tilde{\theta}_t - \theta)}{\sin(\tilde{\theta}_t + \theta)}. \tag{6}$$

In the optical region, due to the high frequency of the impinging radiation, the most general samples are considered as multilayered systems. In such a case, the light transmitted through an interface can be reflected again by the next interface (Fig. 2). This leads to the creation of an infinite series of less and less intense waves due to subsequent reflections, which form the resulting reflected wave.

Starting from the Fresnel coefficients for the single interface, it is useful to derive the total reflection coefficients for the case of film on a substrate:

$$\tilde{R}_p = \frac{r_{p12} + r_{p23}e^{-i2\beta}}{1 + r_{p12}r_{p23}e^{-i2\beta}}; \quad \tilde{R}_s = \frac{r_{s12} + r_{s23}e^{-i2\beta}}{1 + r_{s12}r_{s23}e^{-i2\beta}}, \tag{7}$$

where r_{pij} and r_{sij} represent the reflection terms for p- and s-polarized components, respectively, at each interface:

$$\beta = 2\pi\frac{d}{\lambda}\tilde{N}_2(\omega)\cos\theta_t, \tag{8}$$

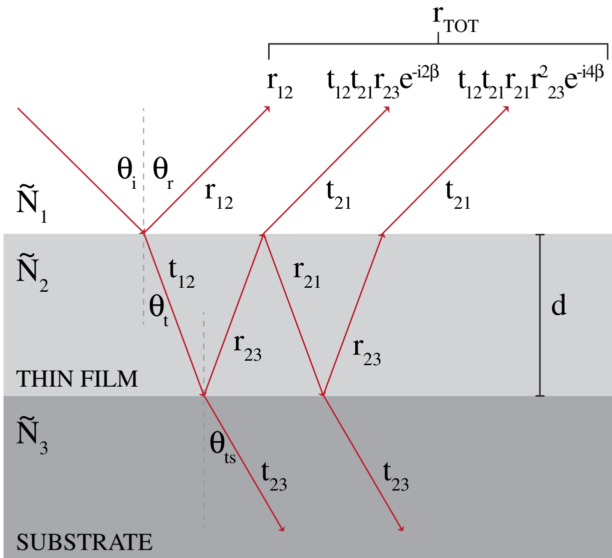

Fig. 2. Pattern of reflections and refractions within a thin film of thickness d. The resultant reflected beam is made up of the initially reflected beam and the infinite series of beams transmitted from medium 2 back to medium 1.

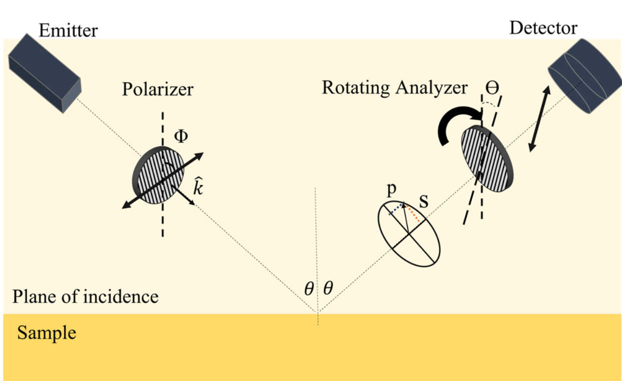

Fig. 3. Sketch of an optical ellipsometer setup with a rotating analyzer (RAE).

expressing the change in the wave phase due to passage through the thickness d of the film [10].

Ellipsometric measurements can be performed as a function of wavelength and angle of incidence. We refer to this configuration as variable angle SE.

A conventional optical setup is usually composed of a source and a detector, with two polarizers in between: input P and analyzer A. Different configurations foresee the possibility for P or A to rotate. Let us take the case of rotating analyzer ellipsometry (RAE), which is one of the most popular configurations (Fig. 3).

In the case of unpolarized or partially polarized light, the general Stokes–Mueller formalism must be used, whereas fully polarized light can be treated with the simpler Jones vector representation [10]. In the following, we will refer to the latter to derive the ellipsometric parameters, since most of the commonly used THz time-domain systems operate with linearly polarized light (see Section 5).

Vector unit $\hat{\mathbf{s}}$, vector unit $\hat{\mathbf{p}}$, and the direction of beam propagation $\hat{\mathbf{k}}$ (in this order) define a right-handed Cartesian reference system. We can therefore express any fully polarized beam through its s and p components and conveniently write them in terms of the Jones vector

$$\begin{bmatrix} \tilde{E}_p \\ \tilde{E}_s \end{bmatrix} = \begin{bmatrix} E_p e^{i\phi_p} \\ E_s e^{i\phi_s} \end{bmatrix}. \tag{9}$$

Let us now use Jones formalism to obtain measured quantities Ψ and Δ in terms of the sample optical properties and the azimuthal angles of the polarizer and analyzer. In this regard, we need to calculate the intensity I_D of the beam reaching the detector as a function of time, which is proportional to the square module of the electric vector field as $I_D \propto |E_D|^2$. In Jones formalism, each optical element acting on the polarization or on the phase terms of the electric field corresponds to a 2×2 matrix. The electric field reaching the detector is therefore given by the product

$$E_D = [\text{Analyzer}][\text{Sample}][\text{Polarizer}][\text{Input}]. \tag{10}$$

To obtain the Jones vector relative to the beam incident on the sample, the coordinate system $s - p$ is rotated with the main axis of the polarizer coincident with the p axis, so that the beam exiting the polarizer is p polarized. Then, through a rotation, one can return to the $s - p$ coordinate system of the ellipsometer. If Φ is the angle between the main axis of the polarizer and the plane of incidence, the Jones vector relative to the beam incident on the sample is given by the product between the rotation matrix of the angle Φ and the Jones vector relative to a p-polarized input beam:

$$\begin{bmatrix} \cos\Phi & -\sin\Phi \\ \sin\Phi & \cos\Phi \end{bmatrix} \begin{bmatrix} 1 \\ 0 \end{bmatrix}. \tag{11}$$

We will analyze the simplest case of an isotropic material, for which the Jones matrix relative to the sample will have zero off-diagonal elements:

$$\begin{bmatrix} \tilde{R}_p & 0 \\ 0 & \tilde{R}_s \end{bmatrix}. \tag{12}$$

For the same reasoning done previously, the Jones matrix for the analyzer is given by the product of a Jones matrix for a linear polarizer with the main axis along the p axis and a rotation matrix of angle Θ between the main axis of the analyzer and the plane of incidence:

$$\begin{bmatrix} 1 & 0 \\ 0 & 0 \end{bmatrix} \begin{bmatrix} \cos\Theta & -\sin\Theta \\ -\sin\Theta & \cos\Theta \end{bmatrix}. \tag{13}$$

Substituting into Eq. (10), we obtain

$$E_D = \begin{bmatrix} 1 & 0 \\ 0 & 0 \end{bmatrix} \begin{bmatrix} \cos\Theta & -\sin\Theta \\ -\sin\Theta & \cos\Theta \end{bmatrix} \begin{bmatrix} \tilde{R}_p & 0 \\ 0 & \tilde{R}_s \end{bmatrix} \begin{bmatrix} \cos\Phi & -\sin\Phi \\ \sin\Phi & \cos\Phi \end{bmatrix} \begin{bmatrix} 1 \\ 0 \end{bmatrix}, \tag{14}$$

which can be easily simplified as

$$E_D = \begin{bmatrix} \tilde{R}_p \cos\Phi \cos\Theta + \tilde{R}_s \sin\Phi \sin\Theta \\ 0 \end{bmatrix}. \tag{15}$$

Finally, by evaluating the square module and rewriting it as a function of parameters Ψ and Δ, we obtain

$$I_D \propto |E_D|^2 = 1 + \frac{\tan^2\Psi - \tan^2\Phi}{\tan^2\Psi + \tan^2\Phi}\cos(2\Theta) + \frac{2\tan\Psi\cos\Delta\tan^2\Phi}{\tan^2\Psi + \tan^2\Phi}\sin(2\Theta). \quad (16)$$

This expression corresponds to the Fourier series for the angle 2Θ:

$$I_D \propto 1 + \alpha\cos 2\Theta + \beta\sin 2\Theta, \quad (17)$$

where α and β are the Fourier coefficients of the signal. If we indicate with f_0 the rotation frequency of the analyzer, angle Θ will be a harmonic function of time:

$$\Theta(t) = 2\pi f_0 t + \Theta_0. \quad (18)$$

Then, having measured I_D, the Fourier transform of the signal is carried out to obtain α and β, from which the relations are inverted to yield the ellipsometric parameters

$$\tan\Psi = \sqrt{\frac{1+\alpha}{1-\alpha}}\,|\tan\Phi|, \quad (19)$$

$$\cos\Delta = \frac{\beta}{\sqrt{1-\alpha^2}}\frac{\tan\Phi}{|\tan\Phi|}. \quad (20)$$

In optical ellipsometry, it is essential to correctly set the measurements and choose an appropriate dielectric function to describe the material under test in the model. To give an example of what can be measured, let us use as a case study indium tin oxide (ITO) [5]. We analyzed a 100 nm thick ITO film coated on 1 mm BK7 glass substrate using a Wollam VASE apparatus. Spectroscopic ellipsometric analysis was carried out in the range of 400–1700 nm at three different angles of incidence, $\theta = 50°$, $55°$, and $60°$, in the vicinity of the material Brewster's angle θ_B ($\approx 63°$). The model consists of three layers: air, ITO, and glass, and the optical response of the ITO layer can be described using two Lorentz oscillators. The good match between experimental and theoretical data is shown in Fig. 4(a). Data inversion analysis provides a spectral curve for each optical constant, n and k [Fig. 4(b)]. Ellipsometry therefore allows to characterize the dielectric function of ITO as a function of wavelength. This is an essential step for the integration of this material in photonic devices.

3. ELLIPSOMETRY IN THE THz RANGE

The previous equations are the basis of ellipsometric measurements for an ellipsometer with a rotary analyzer. Optical ellipsometry data analysis, besides being strongly linked to the specific setup used, must rely also on a specific optical model.

As will be better shown in the following, THz ellipsometry in the time domain can provide direct information on the dielectric response of different materials in solid or liquid form since it is based on a coherent detection technique. By measuring the beam temporal profile impinging on the sample surface and using fast Fourier transform (FFT), both amplitude and phase

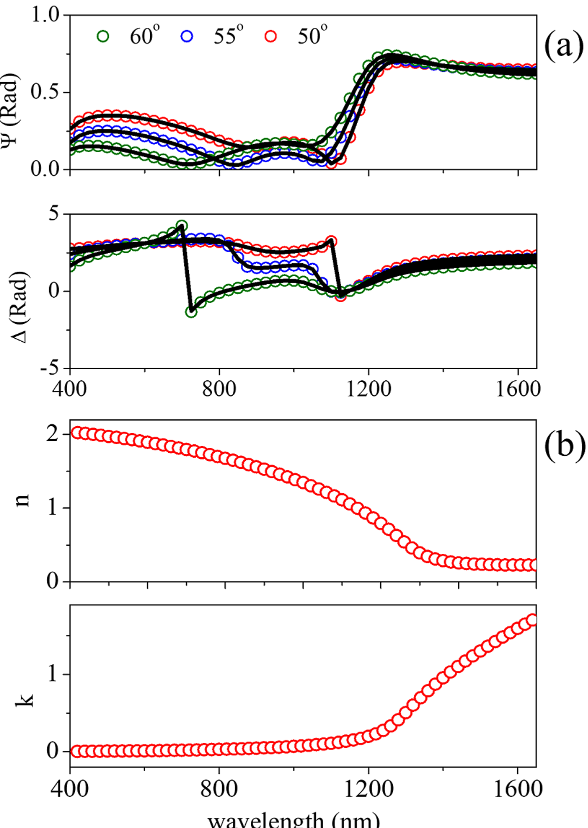

Fig. 4. (a) Ellipsometric spectra (Ψ, Δ) taken at three different angles for a ITO 100 nm thin film deposited on 1 mm BK7 glass substrate. Open circles represent the experimental data, whereas continuous curves describe the theoretical results adopting a three layer model. (b) Optical constants n and k as a function of wavelength obtained using data inversion.

of the signal are independently acquired, and from here, the ellipsometric parameters can be simply measured as a function of frequency.

The terahertz range lies between the microwave and infrared bands, and systems operating in this frequency window usually combine photonic and electronic approaches to generate and detect broad electromagnetic radiation [11]. The corresponding energy is in the range of 10^{-22} to 10^{-20} J, which is associated with the energy of many important chemical and physical processes [12]. Strong absorption lines in the THz spectrum are related to changes in the energy states of vibrational and rotational levels of molecules, providing therefore a specific signature for many materials [13]. Moreover, the sub-mm nature of the wavelength and the relatively high penetration depth of the THz radiation in many materials make it suitable for precision imaging, nondestructive testing, and process quality control [14,15].

As the involved physical processes are different in the THz region, expanding the ellipsometry operational frequency window to smaller energies enables to explore complex phenomena such as spin oscillations [16], anti-ferromagnetic resonances [17], transport in ferroelectrics [18], and free charge carrier oscillations [19], and to fully characterize active and passive polarization sensitive devices such as metasurfaces [20].

Additionally, THz ellipsometry might successfully operate as a characterization technique for the study of challenging materials such as polar fluids or highly conducting thin films and multilayers grown on a dielectric substrate.

Devices and systems working as THz sources were difficult to obtain until recent developments in lasers, quantum wells, and compound semiconductor technology [21]. By the improvement of electronics working in this frequency range [22], spectroscopic techniques have also started to thrive. The increasing interest in THz characterization is due to its potential for accurate and precise extraction of sample optical properties [23], which in principle might shed light on the underlying physical mechanisms. Moreover, a better comprehension of THz radiation–matter interaction leads in turn to an improvement in the design, manufacturing, and operation of THz systems, such as emitting and detecting devices [24–26] for use in novel sensing and communication applications.

In the following subsections, before deepening the description of time-domain ellipsometry, we provide a short overview of the most effective broadband THz generation and detection techniques along with the basics of THz spectroscopy.

A. THz Generation

In conventional techniques, the generation of a coherent THz signal is based mainly on the conversion of a laser pulse with femtosecond duration into a picosecond pulse, which is then Fourier transformed into a broadband frequency spectrum. A large variety of THz emitters are currently in use, and can be divided roughly into two main categories, depending on the underlying mechanism. The first group is based on the induction of a short current pulse in a photoconductive medium, whereas the second group includes systems where generation of THz radiation is realized through nonlinear optical rectification. Due to the cost efficiency, fast response, and easy handling and adjustment to different experimental configurations, a photoconductive antenna (PCA) is the most frequently used source and represents the basic component of many THz spectroscopy and imaging systems. It consists of a photoconductive substrate on which a DC biased metal dipole antenna is patterned. To achieve a broad frequency bandwidth, photoconductive materials with sub-picosecond carrier lifetimes are proposed, among which low temperature grown gallium arsenide (LT-GaAs) is the most common one [27]. To generate THz radiation, an ultrafast laser source, having wavelength usually ranging between 800 and 1500 nm and emitting short pulses with a duration of tens or hundreds of fs, is required. As illustrated in Fig. 5, when a femtosecond pulse illuminates the antenna gap it propagates through the substrate and is absorbed generating photocarriers. A DC biased field accelerates the photocarriers, producing a current that moves through the dipole antenna and re-emits a longer (≈ps) THz pulse.

Recently, accelerator-based and free electron laser (FEL)-based sources are also gaining attention for generating coherent high field THz radiation. A detailed study is presented in [28].

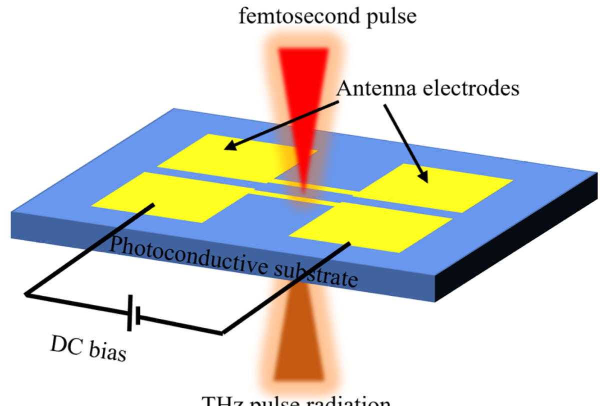

Fig. 5. Photoconductive antenna scheme. The fs laser beam illuminates the photoconductive substrate in the very center of the biased antenna gap, producing a photocurrent and longer (THz) pulsed radiation.

B. THz Detection

PCAs can also be used to detect the THz signal in a coherent manner. To this aim, the driving laser optical pulse is divided into two paths, the pump and the probe arm, to generate and sample the THz signal, respectively. In the detection arm, no external bias is applied. The emitted THz pulse is incident on the PCA and induces a transient bias voltage across the antenna gap passing through the substrate. The measurement of the transient voltage is based on sampling the THz radiation with the fs optical pulse, which is focused on the semiconductor gap and generates free carriers leading to an increase in device conductivity. A current is produced directly proportional to the THz electric field and of the order of nano- to pico-ampere; therefore, its measurement requires selective techniques such as lock-in-amplification. The time profile of the THz beam can be recorded based on two conditions: (i) the detector is sensitive only when the probe and pump beams arrive simultaneously on the detector gap; (ii) the laser beam has a pulse duration much shorter than the THz beam. An optical delay unit provides a time difference between probe and pump beams continuously changing over time and allowing to sweep a pre-defined temporal window, so that the PCA detector can measure the convolution of the laser pulse and the (much longer) THz signal. Figure 6 illustrates how the pump–probe mechanism allows to record the electric field of the THz pulse in a time window through the variable delay unit. The data collected in the time domain can be subsequently converted into the frequency domain through FFT signal processing, providing in such a way direct information on the amplitude and phase of the THz signal [see Figs. 7(a) and 7(b), respectively]. The strong absorption peaks observed in the frequency amplitude spectrum of Fig. 7(a) (continuous black curve) are due to the presence of water vapors in the environment. To mitigate or remove them, measurements need to be carried out in a controlled environment with nitrogen or dry air (dashed red curve). The observed linear behavior in Fig. 7(b) is the result of the phase unwrapping used to avoid discontinuity artifacts (see, for example, [29]). Resolution in the frequency domain relates to the temporal window set in the time-domain signal measurement. The longer the scan,

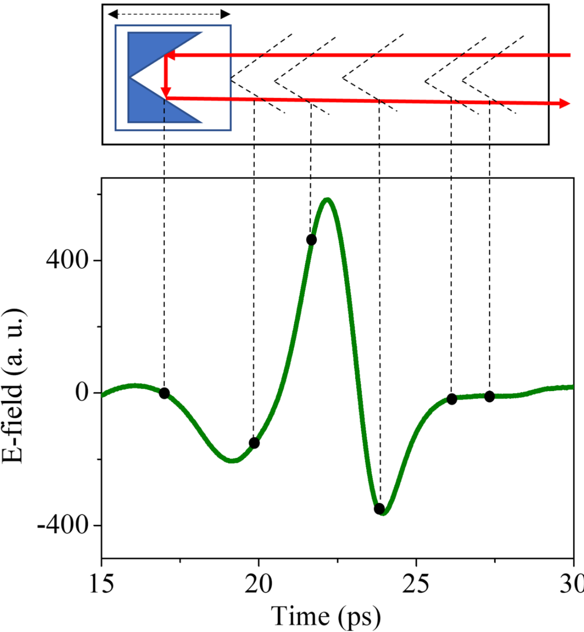

Fig. 6. Sketch of the optical delay unit used in the pump–probe scheme to record the time profile of the THz pulse shown (in arbitrary units) in the graph. Black dots represent the time conversion of the laser beam sampling the ps signal emitted by the PCA.

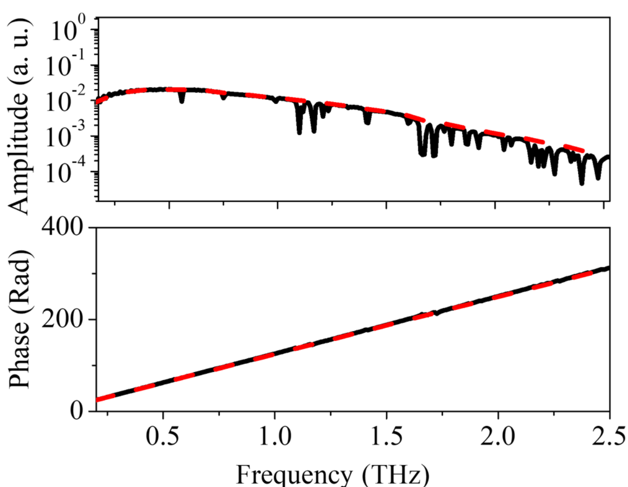

Fig. 7. (a) Amplitude (in arbitrary units) of the time-domain signal converted into the frequency domain using FFT and recorded under ambient (continuous black curve) and dry (dashed red curve) environments. (b) Corresponding phase spectrum (in radians).

the better resolution achieved in frequency, at the expense of increased acquisition time.

C. THz Time-Domain Spectroscopy

THz time-domain spectroscopy (TDS) probes the optical properties of a material using short pulses. This is achieved by comparing in amplitude and phase a reference signal with the electric field after interaction with the sample under test.

The complex transfer function of any material can be expressed as

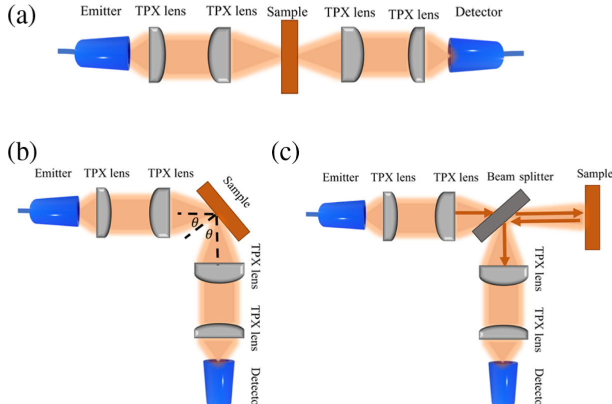

Fig. 8. Sketch of a typical THz-TDS setup in (a) transmission, (b) angular, and (c) specular reflections using fiber coupled antennas.

$$\tilde{T}(\omega) = \frac{\tilde{E}_{\text{sample}}(\omega)}{\tilde{E}_{\text{ref}}(\omega)}, \quad (21)$$

where $\tilde{E}_{\text{sample}}(\omega) = |\tilde{E}_{\text{sample}}|e^{i\phi_{\text{sample}}}$ and $\tilde{E}_{\text{ref}}(\omega) = |\tilde{E}_{\text{ref}}|e^{i\phi_{\text{ref}}}$ represent the THz electric field with and without the sample, respectively. The complex transfer function correlates with the optical properties of the material through the following relations [30]:

$$\ln(|\tilde{T}(\omega)|) = \ln\left[\frac{4n_s}{(1+n_s)^2}\right] - k_s\frac{\omega d}{c}, \quad (22)$$

$$\arg(\tilde{T}(\omega)) = -[n_s - 1]\frac{\omega d}{c}, \quad (23)$$

where c is the light velocity, and n_s, k_s, and d are the refractive index, extinction coefficient, and thickness of the sample, respectively. Equation (22) describes the effect of absorption on the amplitude of the THz signal in the presence of a sample. Equation (23) shows how the refractive index of a sample alters the phase of the THz pulse.

THz-TDS techniques can be applied in both transmission and reflection configurations (see Fig. 8). In the standard measurement setups, the electric field signal generated by the emitter PCA is first collimated and then focused on the sample surface using lenses transparent in the THz range (such as TPX, polymethylpentene, a crystalline polymer) or off-axis metallic parabolic mirrors. After being transmitted/reflected, the signal modified by the material interaction—using a reverse optical scheme—reaches the detector PCA. Material parameter extraction is straightforward in both transmission and (normal) reflection geometries. Nevertheless, THz-TDS in a transmission configuration is limited within the skin depth for relatively thick, highly doped, and/or conductive materials. Similarly, it is not possible to apply the technique in the case of highly absorptive media such as polar liquids. Under these conditions, one can resort to reflection measurements, which however, suffer from technical limitations and errors in sample–reference relative positioning, leading to a high uncertainty in the extracted material parameters [31].

4. COMBINING THz-TDS AND ELLIPSOMETRY

As stated earlier, the advantage of time-domain THz spectroscopic systems is that the signal is *coherently* detected. Moreover, different from standard transmission or (specular/variable) reflection methods, ellipsometry is a self-reference technique and avoids errors related to reference and sample relative misplacement. Therefore, in removing inherent limitations of TDS transmission and overcoming errors stemming from TDS reflection, time-domain THz ellipsometry can combine the best of both worlds, acquiring reliable information on both intensity and phase of the reflected signals and providing direct measurement of ellipsometric parameters.

TDS ellipsometry (TDSE) directly measures the time dependent electric field of the signal. Applying Jones analysis to retrieve ellipsometric angles is not necessary, since the amplitude ratio and the phase difference are simply extracted from time-domain signals using Fourier transform.

Basically, the temporal profile of the electric field p- and s-polarized components interacting with the sample surface are separately detected. Then, through FFT analysis, the time-domain data related to each polarization state are transformed into the frequency domain to give the amplitude and phase of the polarized signals after reflection. In such a way, one can extract in a straightforward manner Ψ and Δ from Eqs. (1) and (2). In comparison with standard transmission spectroscopy, however, the separate detection of the p and s signals can be a limit under specific circumstances (close to the Brewster's angle).

Using Eqs. (5) and (6), after some simple math, the constitutive relations linking the refractive index (real part) n and the absorption coefficient k of the material under investigation to the experimentally determined quantities Ψ and Δ (and the angle of incidence θ) can be obtained [32]:

$$n^2 - k^2 = \sin^2\theta \left[1 + \frac{\tan^2\theta(\cos^2 2\Psi - \sin^2 2\Psi \sin^2\Delta)}{(1 + \sin 2\Psi \cos\Delta)^2}\right], \quad (24)$$

$$2nk = \sin^2\theta \frac{\tan^2\theta \sin 4\Psi \sin\Delta}{(1 + \sin 2\Psi \cos\Delta)^2}. \quad (25)$$

A. Dependence of the Ellipsometric Parameters on Incidence Angle

By using Eqs. (24) and (25), one can investigate how the ellipsometric parameters behave when varying the angle of incidence at a given frequency. Since different materials have different Ψ and Δ angular dependence, a simple θ scan can be used to preliminarily investigate the sample characteristics. Furthermore, in the case of materials having well-known properties, the comparison of the experimentally measured angular dependence of ellipsometric parameters with theoretical expectations can be exploited to check the correct setting of the incident angle itself.

For instance, Fig. 9 plots the angular dependence of Ψ and Δ for some representative materials: (a) a low loss insulator (high resistivity single crystalline silicon plate), (b) an absorptive dielectric medium [ultra-pure deionised (Milli-Q) water], and (c) an almost perfect conductor (gold thick film) at 0.4 THz.

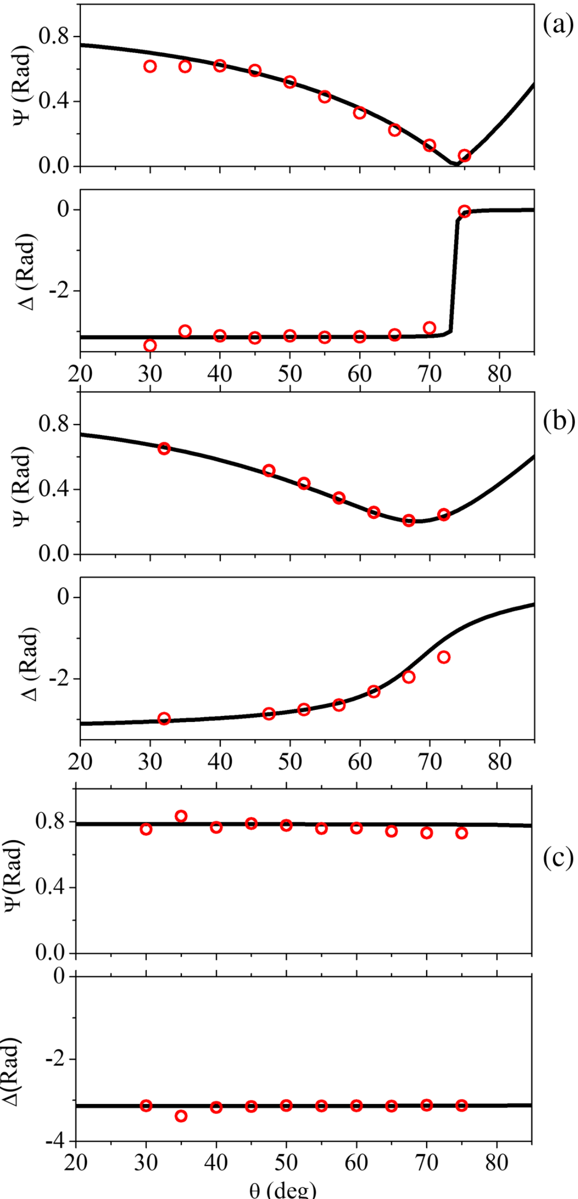

Fig. 9. Comparison between experimental values (red full circles) and theoretical expectations (black continuous curves) of Ψ and Δ versus θ at 0.4 THz in (a) high resistivity single crystal silicon, (b) ultra-pure deionized (Milli-Q) water, and (c) gold thin film.

The continuous black curves describe the theoretical behavior predicted using Eqs. (24) and (25), and the red circles the experimental values taken at different incident angles using a well-calibrated THz ellipsometer.

As illustrated in Fig. 9(a), for the insulator, Ψ goes to zero, and Δ changes the sign at the corresponding Brewster's angle ($\theta_B \approx 74°$ for Si), as expected for a material with losses virtually close to zero. Conversely, a metal such as gold [Fig. 9(c)] shows a very large reflectivity and a high level of absorption. Ψ is constant to the value 45° independently of the angle of incidence, indicating the equality of the p- and s-polarized component amplitudes reflected from the surface (but very close to the corresponding pseudo-Brewster's angle $\theta_{B'}$, not displayed in the graph). Δ shows a similar behavior, keeping constant for most of

the incident angles and then undergoing a pronounced variation close to $\theta_{B'}$. The case of water [Fig. 9(b)] is an intermediate one, since it has a finite extinction coefficient k with a relatively small refractive index n. In a lossy medium with low reflectivity, the p-polarized component in comparison with the s-polarized goes through a non-zero minimum approaching the corresponding pseudo-Brewster's angle ($\theta_{B'} \approx 65°$ for water); therefore, Ψ never goes to zero. Δ shows also a smoother variation with respect to the first case.

The good agreement between experimental data and theoretical expectations for all three samples shows the robustness of the ellipsometric setup and a great deal of confidence in the setting of incidence/reflectance angles, which is extremely important, especially in the vicinity of θ_B or $\theta_{B'}$.

B. Effect of Measurement Errors on the Determination of Optical Constants

In time-domain methods, there is always an uncertainty in recording the transient electric field transmitted and detected by the antennas. Additionally, in fiber-coupled THz systems, phase shift errors due to fiber sensitivity to small deviations in temperature or external vibrations are possible [33,34]. These effects must be taken into account since they can deteriorate the precision in ellipsometric measurements.

Defining $\delta|\tilde{E}|$ and $\delta\phi$ as the uncertainty in amplitude and phase, respectively, of the electric field recorded by the detector, from Eqs. (1) and (2), one can easily evaluate the errors $\delta\Delta = \sqrt{2}\delta\phi$ and $\delta\Psi = \frac{\tan(\Psi)}{1+\tan^2(\Psi)}\left(\frac{\delta|\tilde{E}_p|}{|\tilde{E}_p|} + \frac{\delta|\tilde{E}_s|}{|\tilde{E}_s|}\right)$ in the ellipsometric parameters.

From these expressions, one can observe that while $\delta\Delta$ is directly proportional to the error $\delta\phi$ in phase measurements and therefore has no angular dependence, $\delta\Psi$ is related to both $\tan(\Psi)$ and the relative errors in the determination of amplitude for the p- and s-polarized electric fields reaching the detector. All these terms are strongly dependent on θ (see Fig. 9).

Predicting how measurement errors modify the accuracy in the evaluation of n and k is definitively less obvious, since one has to evaluate the effect of the uncertainties $\delta\Delta$ and $\delta\Psi$ in the constituent relations Eqs. (24) and (25). This effect can be empirically investigated by applying a pre-determined variation to the values of the ellipsometric parameters and studying how it translates into a change of optical constants for different incident angles. Figure 10 shows how a small uncertainty in Ψ or Δ can affect the way the optical properties are extracted from ellipsometric measurements when varying θ, in single crystal Si [Figs. 10(a) and 10(b)] and in ultra-pure deionized (Milli-Q) water [Figs. 10(c) and 10(d)]. The relative deviations $\frac{\delta n}{n}$ and $\frac{\delta k}{k}$, defined as the normalized difference between the values estimated from Eqs. (24) and (25) and the one experimentally obtained from highly precise standard spectroscopy measurements, are displayed. In (a) and (c), a variation $\pm 0.5°$ ($\approx$10 mRad) is applied to Ψ, while Δ remains unchanged. To the contrary, (b) and (d) show results for $\Delta \pm 0.05°$ ($\approx$1 mRad) while keeping Ψ constant.

For silicon, being a low loss material, the behavior observed in the corresponding graphs confirms [10] that variations in $\Psi(\Delta)$ significantly affect changes in $n(k)$ only. The sudden increase

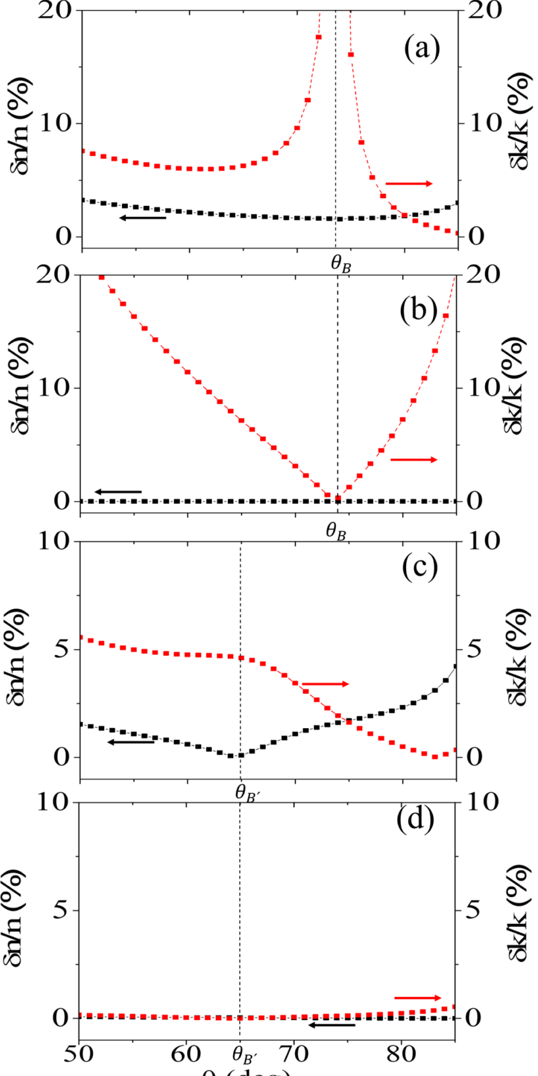

Fig. 10. Relative deviation (in percentage) $\frac{\delta n}{n}$ and $\frac{\delta k}{k}$ of the complex refractive index for silicon and water estimated through the ellipsometric parameters with respect to reference values yielded using TDS, at 0.4 THz, and varying the beam incident angle. (a), (c) $\Psi \pm 0.5°$, Δ constant. (b), (d) $\Delta \pm 0.05°$, Ψ constant. The Brewster's angle θ_B for silicon and pseudo-Brewster's angle $\theta_{B'}$ for water are indicated in the graphs with dashed vertical lines.

in $\frac{\delta k}{k}$ observed in Fig. 10(b) very near the Brewster's angle has to be ascribed to Ψ going to zero, making the value of k undetermined in correspondence of θ_B. In spite of this, the common feature of Figs. 10(a) and 10(b) is that accuracy increases near the Brewster's angle, indicating the importance in ellipsometric measurements of a setup capable to operate in close proximity.

In the case of water and more generally for samples with a significant absorption, since both Ψ and Δ have a smoother angular dependence [see Fig. 9(b)], changes in n and k are less dependent on the proximity to $\theta_{B'}$ [Fig. 10(c)], or are not sensitive at all [Fig. 10(d)]. It is worthwhile to observe that for a lossy material, the accuracy in the evaluation of k particularly improves with respect to the almost transparent silicon.

5. THz ELLIPSOMETRY SETUP AND CALIBRATION

THz ellipsometry is a relatively young field. Presently, because of the larger wavelengths involved, any setup is very sensitive to the focusing and matching conditions of the electroptical components (antennas, lenses, polarizers). Therefore, system architecture and strategies for optical alignment and calibration are usually more challenging than in the optical region and represent an open area of discussion among scientists.

The first ellipsometer operating in the THz region was proposed in 2010 by Hoftman *et al*. [35]. It consists of backward wave oscillators (BWOs) acting as sources and a Golay cell used for signal detection. The system is based on a polarizer-sample-rotating compensator–analyzer arrangement [36]. The polarization control elements are a variable odd bounce image rotation system in combination with a wire grid polarizer (WGP) in the emitter arm and a rotating analyzer in the detector arm. The sample stage is placed on a high precision $\theta - 2\theta$ goniometer, allowing variable incident angle measurements (from 30° to 90°). In 2018, Kuhne *et al*. [37] designed a similar system with further developments, including solutions from stealth technology to suppress speckle and reduce standing wave formation, the addition of bolometers along the detection arm, and the possibility of *in situ* experiments on samples exposed to different gaseous environments in a cryostat under a high (8 Tesla) magnetic field. Use of BWOs as sources of radiation and bolometer detectors or Golay cells as THz detectors provides a wavelength tunable ellipsometer, directly working in the frequency domain (0.1–1.5 THz) with a very high frequency resolution, of the order of MHz. Very recently, a compact and lightweight portable spectroscopic quasi-optical ellipsometer–reflectometer (SQOTER), consisting of two channels with a common emitter, was reported [38,39]. The authors use different frequency sources to cover the sub-THz range (0.1 to 1 THz) and a pre-amplified detector connected to a scalar network analyzer to measure the signal amplitude. Other frequency domain systems use instead the THz radiation emitted from a FEL as a light source [40].

All the aforementioned setups, however, represent non-coherent spectroscopic techniques and therefore, as they are, do not exploit the full potential of time-domain measurements. In 2013, Neshat and Armitage [41] reported the first multi-angle THz ellipsometer ($15° < \theta < 90°$) operating in the time domain, in which the emitter arm is fixed to the optical table and the detector arm is free to move. A sample is placed on a rotating stage to provide symmetry between incident and reflected angles. PCAs are used for both THz generation and detection. To eliminate the uncertainties in polarization response as well as the errors in the angular setting, a calibration scheme for a rotating element optical ellipsometer is adopted [42]. In 2014, Yamashita *et al*. [43] proposed a THz ellipsometer working at a fixed angle of incidence ($\theta = 60°$) with a broad frequency band coverage (0.5–30 THz). Basing on optical rectification effects, GaP and GaSe crystals excited by a femtosecond laser with an 800 nm center wavelength are used as sources of THz-MIR radiation, whereas an LT-GaAs epitaxial layer-transferred photoconductive switch (ELT-PCS) is chosen as the system detector. Ultra-broadband polarizers are inserted into the optical path to control/analyze the p- and s-polarized components of the generated/reflected pulses. Recently, Chen *et al*. [44] proposed an all fiber-coupled PCA-based THz ellipsometer with a third polarizer added to compensate for time shift errors, optical mismatches, and imperfections in antenna responses. Calibration of the system is done using a complicated algorithm based on interference theory. Instead of an optical polarizer, Baez-Chorro *et al*. [45] introduced into their setup a birefringent medium to time delay the two orthogonal polarizations of the THz signal. The introduction of a phase shift allows to eliminate the analyzer and simplify measurements. However, since the time-domain signal for each electric field component must be "windowed," this limits the accuracy in the frequency response for each polarization component. A different approach was proposed by Guo *et al*. [46]. By combining the mechanical rotation of a wire grid with a quadrature-phase detection method, they presented a new setup for THz ellipsometric measurements in the time domain that is capable of simultaneously measuring s- and p-polarization components with no need for a rotating polarizer. Very recently, Agulto *et al*. [47] in collaboration with Nippo Precision, Co., Ltd. developed a commercial system for THz ellipsometry measurements (0–4 THz) in the time domain (Tera Evaluator) that is capable of measuring carrier density, mobility, resistivity, and thickness of bulk semiconductors, in addition to dielectric properties of many materials. To reduce systematic errors from the signals, the system performs multiple analyzer azimuthal angle measurements. It is also worth mentioning the work done by Marsik *et al*. [48], which developed an ellipsometer covering a very wide frequency band (0.1–21 THz). In the low THz range, they use a home-built system operating in the time domain.

Table 1 summarizes the main studies reported in literature on THz ellipsometry. It is worth mentioning that different or mixed methods of THz generation and coherent detection can be employed, provided that the detector shows a bandwidth greater than or equal to the emitter.

In the following subsections, the discussion will focus on the TDSE developed at the Department of Physics of the University of Naples "Federico II" and operating in the range of 0.1–0.6 THz. We first explain the main components and the optical setup of a fiber coupled THz ellipsometer operating in the time domain. Subsequently, we briefly introduce the necessary steps for accurate calibration, by using a fast and effective algorithm-assisted compensation technique. At the end, to verify the process, we report the ellipsometric measurements carried out on solid and liquid samples at different incident angles. The retrieved complex dielectric properties of the samples under test are compared, whenever possible, with the same parameters obtained using the standard THz spectroscopy analysis.

A. Customized THz-TDSE Setup

Figure 11 displays the schematic representation (a) along with a picture (b) of the TDSE setup. The THz ellipsometric system shown is basically based on the implementation of a standard time-domain spectrometer in transmission mode. The source for THz generation is a femtosecond laser with pulse duration less than 150 fs. The ellipsometer is equipped with fiber coupled PCAs and independent arms, providing more flexibility during measurements and the capability to switch with ease to

Table 1. Characteristics of Different THz Ellipsometer Setups

Group	Emission	Detection	Frequency Range	Operation Domain
Hoftman *et al.* [35]	BWO	Golay cell	0.2–1.5 THz	Frequency domain
Kuhne *et al.* [37]	BWO	Golay-cell/FTIR	0.1–1 THz	Frequency domain
Neshat and Armitages [41]	PCA	PCA	0.1–1.5 THz	Time domain
Yamashita *et al.* [43]	GaP/*z*-cut GaSe crystal	ELT-PCS	0.5–30 THz	Time domain
Chen *et al.* [44]	PCA	PCA	0.2–1.6 THz	Time domain
Baez-Chorro *et al.* [45]	PCA	PCA	0.2–1 THz	Time domain
Agulto *et al.* [47]	PCA	PCA	1–3 THz	Time domain
Belyaeva *et al.* [39]	BWO	Amplitude detector	0.1–1 THz	Frequency domain
Marsik *et al.* [48]	PCA	Laser Quantum Tera-SED	0.1–21 THz	Time domain
Guo *et al.* [46]	PCA	PCA	0.1–1.5 THz	Time domain

(a)

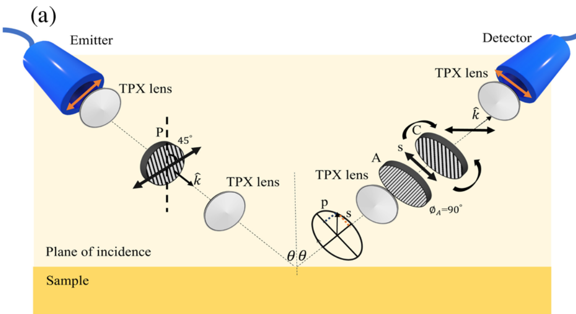

(b)

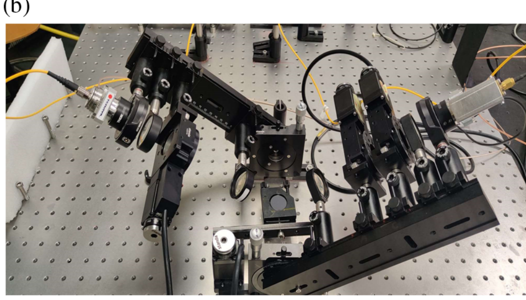

Fig. 11. (a) Sketch and (b) picture of the fiber-coupled THz opto-mechanical system for ellipsometric measurements. In (a), P, A, C stand for the role played by each wire grid polarizer (see text).

the standard transmission TDS mode. Moreover, the setup is designed to have the plane of incidence always perpendicular to the optical table, allowing to test liquid samples in a very simple way. Three substrate-free WGPs with broadband transmission and high extinction ratios (between 20 and 50 dB) are used to precisely control the polarization state of incident and reflected waves. Each polarizer has wire diameter 10 μm, wire spacing 25 μm, and an aperture of 15 mm, and is placed on a high precision computer controlled rotational stage.

The emitter arm consists of: (i) a PCA emitting linearly polarized THz radiation and rotated by 45° in the azimuth plane, and (ii) the first polarizer (P) aligned along the electric field direction, with an azimuth angle ϕ_P set at 45° to remove any cross-polarization. In this configuration, the eigenstates (p and s polarized) of the generated THz signal are distinguishable.

On the detector arm, there are: (i) a second polarizer (A) set at $\phi_A = 0°$ or $\phi_A = 90°$ to select p- or s-polarized electric field components only, and a third polarizer (C) used to modify in the time domain their ratio; (ii) the PCA rotated by 45° in the azimuthal plane to detect with the same sensitivity the p- and s-polarized signals reflected from the sample surface.

Although its presence is usually optional in ellipsometric setups, the role of polarizer C is important to compensate for possible errors caused by the imperfect dipolar responses of PCAs, nonplanar wavefront of the THz beam, misorientation of polarizers P and A, or imprecise settings of their azimuthal angles. In the ideal case, compensator C azimuth angle should be kept at $\phi_C = -45°$. In practice, its value may vary—depending also on the incident angle—in a small range centered around $-45°$, and its setting should be precisely determined using the calibration procedure.

In the setup presented in Fig. 11, two different pairs of TPX polymeric lenses are used to collimate and focus the THz signal emitted by the first PCA, impinging onto the sample plane and then received by the second PCA. At the focus point, the beam waist is measured to be approximately 5 mm. The sample is placed on a kinematic platform coupled with two-axis motorized linear stages providing sensitive control of the focusing conditions along with surface parallelism with respect to the beam wavefront. An accurate placement of the sample at the focal length is important to enhance the detection of the signal from the surface, although ellipsometry is less prone to errors stemming from imprecise material positioning with respect to other reflection techniques [37,49]. TPX lenses can be easily replaced by off-axis parabolic mirrors, which introduce no aberrations and less divergence of the THz beam, at the expense, however, of higher complexity in the optical setup.

B. THz-TDSE Setup Calibration

Calibration of a THz-TDSE is the most important and time consuming step toward accurate material parameters extraction. In this respect, some strategies can be adopted in effectively calibrating a variable angle THz ellipsometer operating in the time domain, which are explained in detail in a separate work [50].

Briefly, our approach is based on the comparison in the time domain of the ellipsometric derived s- and p-polarized components of the electric field at a given angle of incidence with the reconstructed ones, attained by using the complex dielectric function of a known sample. The calibrated response is determined with high precision by setting the system in transmission mode.

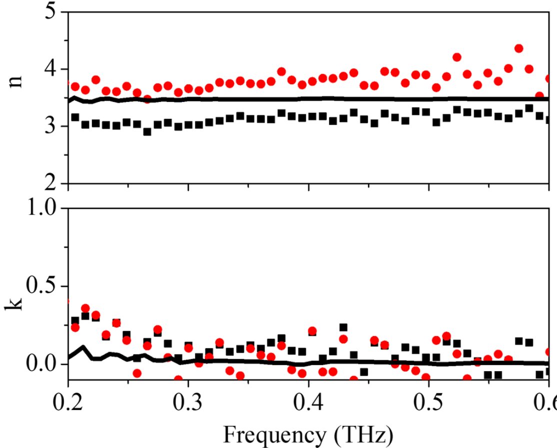

Fig. 12. Optical constants n and k versus frequency for silicon measured using THz ellipsometry at $\theta = 70°$. Black squares describe uncalibrated measurements, whereas red circles represent results of the calibrated setup. The continuous black curves report the values extracted using THz-TDS in transmission configuration.

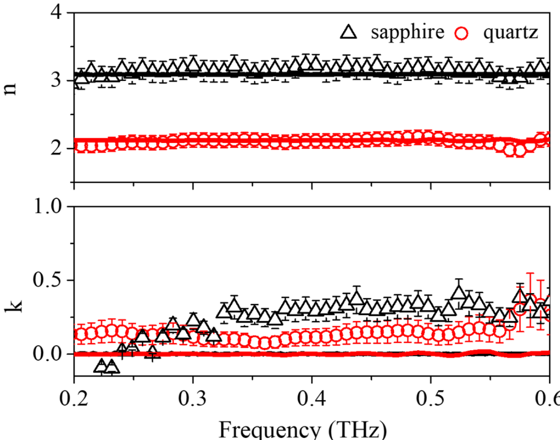

Fig. 13. Optical constants n and k versus frequency for crystalline z-cut quartz (red circles) and single crystal z-cut sapphire (black triangles) measured using THz ellipsometry at $\theta = 60°$. The continuous black and red curves report the corresponding values extracted using THz-TDS in transmission configuration.

Figure 12 presents the results of ellipsometric measurements aimed to yield the complex refractive index of a high resistivity silicon sample before ($\phi_c = -45°$) and after (ϕ_c is modified based on the specific procedure) calibration. The continuous black curves show values extracted using THz-TDS in a transmission configuration and used as a dependable reference. As shown, the proposed calibration scheme improves the precision of THz ellipsometry in retrieving the complex refractive index but for the real part only. Indeed, for transparent and semi-transparent materials, Δ is approximately constant and equals the value π (see Fig. 9), i.e., no phase change is observed between s- and p-polarized components. In such a case, according to Eq. (25), measurements of the extinction coefficient are rather difficult. As a matter of fact, ellipsometry does not perform well in low or near zero absorption materials [10]. Nevertheless, as discussed in the following, its precision increases for highly absorptive materials such as polar fluids.

6. MEASUREMENTS

In previous sections, we cast a glance at the characteristics of THz-TDSE, which promises to be a powerful tool for high precision characterization of a wide range of materials, from opaque bulk samples [51] to multilayered structures [52], liquids, and biological tissues [53]. To examine the reliability of the TDSE technique, it is worthwhile to investigate with ellipsometric measurements some materials in different forms (from bulk to liquid and conducting thin film), as they are a subject of great interest in the THz region.

A. Bulk Materials

The study of optical properties of relatively thick or highly absorptive materials is usually difficult using THz-TDS in transmission mode, due to the skin depth limitation of THz radiation. THz-TDSE represents a suitable and effective alternative.

Figure 13 shows the results of the characterization of bulk materials with the setup presented in Fig. 11, first in a transmission configuration and then in the ellipsometric mode at $\theta = 60°$, using high resistivity silicon as a calibration sample.

Investigated samples are (i) a crystalline quartz, SiO_2, and (ii) a single crystal sapphire, Al_2O_3, having thicknesses $d = 0.4$ mm and 8 mm, respectively. Since both quartz and sapphire are birefringent materials, crystals are chosen to be z-cut (oriented along the ordinary axis) so that changes in polarization produced by the difference between ordinary and extraordinary axes are minimized [54,55] and below the limit of detection of the setup.

As crystalline quartz is a relatively thin sample, we observed the signal reflected from the backside surface in the time-domain data. To reduce oscillations in the FFT spectra, we chose cutting and "zero padding" the time-domain signals. To the contrary, the significantly larger thickness of the single crystal sapphire, while obviating backside reflection effects, significantly reduces the transmitted signal in TDS measurements.

In both samples, there is a remarkable agreement between the frequency dependence of the refractive index evaluated using the two different techniques. As for the extinction coefficient, TDSE slightly overestimates the results obtained using conventional transmission spectroscopy, which we believe is simply indicative of poor sensitivity for k. As already said, ellipsometry is not a suitable characterization technique for the determination of k in materials having small losses, preventing in such cases a reliable extraction of this parameter [10]. It is obvious that information achievable using single surface reflection cannot compare with the accuracy level of transmission, which provides a much better contrast for transparent materials in both phase (two sample surface interactions) and amplitude (energy loss across the entire sample). On the other hand, this highlights the power of the ellipsometry technique in measuring samples that are opaque in the THz region.

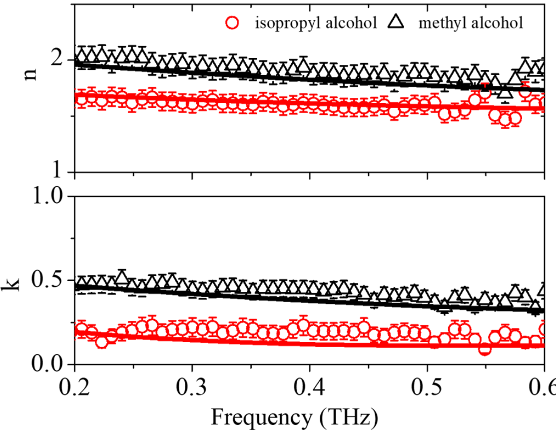

Fig. 14. Optical constants n and k versus frequency for isopropyl alcohol (99.7% purity, red circles) and methyl alcohol (99.8% purity, black triangles), measured using THz ellipsometry at $\theta = 55°$ and 60°, respectively. The continuous black and red curves report the corresponding values extracted using THz-TDS in transmission configuration.

B. Liquids

Characterization of liquids (especially polar fluids) in the THz range is rather challenging since they are usually extremely lossy in this region of the electromagnetic spectrum. THz ellipsometry is therefore a very promising method for studying very absorptive materials. In comparison, TDS measurements in liquids are cumbersome since each time a thin layer (d $\approx$100 µm) of the sample under test is placed inside a cuvette made of quartz (or another semi-transparent material in the THz region), data must be compared with same measurements performed using the blank cuvette.

Having the arm movement perpendicular to the optical table, the proposed TDSE setup can conveniently measure liquids even in large volumes. The experiment precision can increase when the setup is calibrated using ultra-pure deionized (Milli-Q) water. Figure 14 shows the results of experiments done on common polar fluids, isopropyl alcohol (99.7 % purity) and methyl alcohol (99.8 % purity). The ellipsometric measurements were conducted at $\theta = 55°$ and 60° for isopropyl and methyl alcohol, respectively, in the vicinity of $\theta_{B'}$ for each sample. In this case, given the lossy nature of the samples, graphs show an excellent agreement both in n and k with data obtained using the transmission configuration.

C. Thin Films

Characterization of thin films in the THz region is increasingly recognized as a promising research field since they can be effectively used for sensing in many different applications, from the investigation of dynamics in strongly correlated systems to the probing of biological samples [56]. Additionally, the study of thin film properties is required in situations where there is a limitation in the sample volume such as in the case of DNA, toxic, or volatile materials, or preparation is simplified as in the case of biologically active or functionalized chemical monolayers. Moreover, in some cases, samples in thin film form show different THz properties from their bulk counterparts because of surface roughness, grain size, and additional strain stemming from the fabrication process.

Under these circumstances, the use of conventional TDS fails or is heavily hampered by the reduced sensitivity of the technique. For samples having thicknesses of the order of tenths of micrometers, the maximum carrier concentration that can be measured usually does not exceed 10^{19} cm^{-3} [57]. Using TDSE can overcome this limitation; however, the main reflected pulse and the internal reflections coming from a thin film (see Fig. 2) partially overlap in the recorded time signal, making data analysis more challenging than in bulk samples. To retrieve the THz properties of a thin layer deposited on a substrate, a suitable optical model of the whole system is needed, in which the unknown properties of the film under investigation are modeled using a proper response function. For instance, a transparent dielectric material is easily described using a Cauchy dispersion function, whereas for a conducting layer, a generalized Drude model can be employed.

For a multilayer medium, Ψ and Δ are oscillating functions in which the number of oscillations increases with increasing film thickness (d) and refractive index ($\tilde{N}_2$) [10]. Under these conditions, the complex ratio ρ in Eq. (3) is not directly solvable. Nevertheless, since TDSE provides direct access to ellipsometric parameters Ψ and Δ, comparing their experimental values with the calculated counterparts through a nonlinear regression minimization procedure usually allows to retrieve the optical constants of the unknown layer.

For instance, in the case of a thin ITO layer deposited on fused quartz, one can use a three layer (air–ITO–substrate) model, inserting the known properties of SiO_2 and the generalized Drude law (to express the response of the conducting layer only) in the nonlinear regression algorithm. Then, Ψ and Δ are let to vary until they best match the experimentally measured values, as shown in Fig. 15(a) for a 200 nm ITO layer deposited on 1.3 mm fused silica. Fitting parameters are the relaxation time ($\approx 7.2 * 10^{-15}$ s) and the number of carriers ($\approx 2.7 * 10^{20}$ cm^{-3}), yielding a value of the plasma frequency of $1.6 * 10^{15}$ Hz, in excellent agreement with results reported in literature for a similar sample [58]. Since the film thickness is relatively very small, in such a case, the ellipsometric parameters do not display oscillating behavior. Figure 15(b) shows the optical constants retrieved using the fitting procedure. Extracted values well match previous experiments [58], which are shown for comparison as dashed curves in the same graph.

7. CONCLUSION

We have presented a short overview on recent developments in time-domain ellipsometry, which promises to be a powerful technique for the characterization of materials in the THz range. In comparison with its analog in the optical region, a THz ellipsometer benefits from the coherent detection of the beam reflected from the sample surface, making characterization easier since in the case of homogeneous materials, the optical properties of the sample can be directly measured from the ellipsometric parameters. Moreover, conversely to a standard optical RAE, TDSE does not need a continuously rotating element in the apparatus setup. However, due to the larger wavelengths in the region of investigation, calibration of a THz ellipsometer

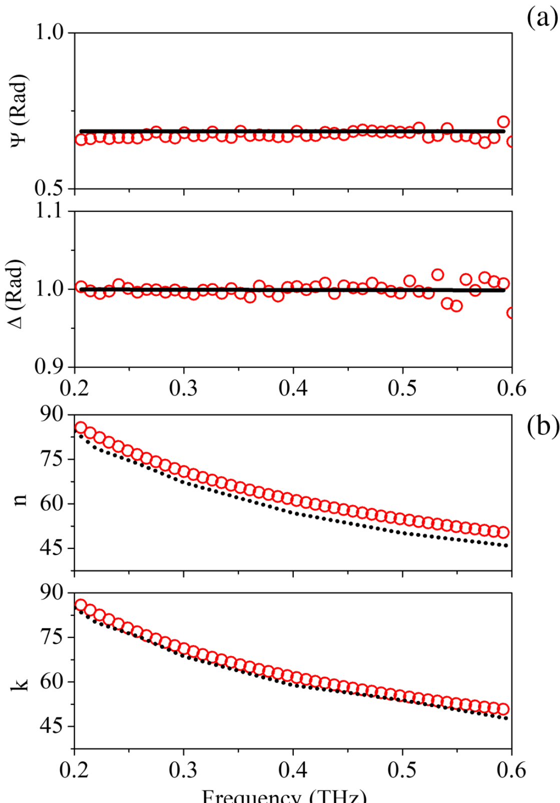

Fig. 15. (a) Ellipsometric angles Ψ and Δ versus frequency for an ITO 200 nm layer deposited on 1.3 mm fused silica substrate. Open circles represent the experimental results, whereas continuous curves refer to the theoretical three layer model (see text). (b) Corresponding optical constants n and k. Dashed lines represent values obtained using standard THz spectroscopy [58].

is challenging, since it has presently to face a complex optical alignment and a beam with non-ideal characteristics. To address these issues, a calibration scheme is proposed that allows to realize fine adjustment of the polarizers' azimuthal angles at each selected incidence angle, compensating for most of the possible errors arising in the experimental setup. The effect on measurement accuracy produced by uncertainties in the determination of amplitude and phase of the polarized electric field components is also discussed. Examples of measurements performed on a wide range of materials such as bulk dielectrics, polar fluids, and thin conducting layers are presented, and data extracted using Eq. (24) and Eq. (25) are compared with values obtained using standard transmission spectroscopy, showing excellent agreement.

Acknowledgment. This work has been conducted under the auspices of INFN Italy and supported in part by the project "TERA."

Disclosures. The authors declare no conflicts of interest.

Data availability. Data underlying the results presented in this paper are not publicly available at this time but may be obtained from the authors upon reasonable request.

REFERENCES

1. P. Drude, "Ueber Oberflächenschichten. I. Theil," Ann. Phys. **272**, 532–560 (1889).
2. P. Drude, "Ueber Oberflächenschichten. II. Theil," Ann. Phys. **272**, 865–897 (1889).
3. A. Rothen, "The ellipsometer, an apparatus to measure thicknesses of thin surface films," Rev. Sci. Instrum. **16**, 26 (1945).
4. R. J. Archer, "Determination of the properties of films on silicon by the method of ellipsometry," J. Opt. Soc. Am. **52**, 970 (1962).
5. V. Tkachenko, A. Marino, F. Vita, F. D'Amore, L. De Stefano, M. Malinconico, M. Rippa, and G. Abbate, "Spectroscopic ellipsometry study of liquid crystal and polymeric thin films in visible and near infrared," Eur. Phys. J. E **14**, 185–192 (2004).
6. A. Marino, G. Abbate, V. Tkachenko, I. Rea, L. De Stefano, and M. Giocondo, "Ellipsometric study of liquid crystal infiltrated porous silicon," Mol. Cryst. Liq. Cryst. **465**, 359–370 (2007).
7. A. Marino, E. Santamato, N. Bennis, X. Quintana, J. Otón, V. Tkachenko, and G. Abbate, "Ellipsometric study of vertically aligned nematic liquid crystals," Appl. Phys. Lett. **94**, 013508 (2009).
8. A. Marino, V. Tkachenko, E. Santamato, N. Bennis, X. Quintana, J. Otãn, and G. Abbate, "Measuring liquid crystal anchoring energy strength by spectroscopic ellipsometry," J. Appl. Phys. **107**, 073109 (2010).
9. V. Tkachenko, G. Abbate, A. Marino, F. Vita, M. Giocondo, A. Mazzulla, and L. De Stefano, "High accuracy optical characterization of anisotropic liquids by merging standard techniques," Appl. Phys. Lett. **89**, 221110 (2006).
10. H. Fujiwara, *Spectroscopic Ellipsometry: Principles and Applications* (Wiley, 2007).
11. X.-C. Zhang and J. Xu, *Introduction to THz Wave Photonics* (Springer, 2010), Vol. **29**.
12. L. Consolino, S. Bartalini, and P. De Natale, "Terahertz frequency metrology for spectroscopic applications: a review," J. Infrared, Millim. Terahertz Waves **38**, 1289–1315 (2017).
13. L. Ho, M. Pepper, and P. Taday, "Signatures and fingerprints," Nat. Photonics **2**, 541–543 (2008).
14. C. Koral, M. Fantauzzi, C. Imparato, G. Papari, B. Silvestri, A. Aronne, A. Andreone, and A. Rossi, "Defects in the amorphous–crystalline evolution of gel-derived TiO_2," J. Phys. Chem. C **124**, 23773–23783 (2020).
15. S. Zhong, "Progress in terahertz nondestructive testing: a review," Front. Mech. Eng. **14**, 273–281 (2019).
16. S. Baierl, M. Hohenleutner, T. Kampfrath, A. Zvezdin, A. V. Kimel, R. Huber, and R. Mikhaylovskiy, "Nonlinear spin control by terahertz-driven anisotropy fields," Nat. Photonics **10**, 715–718 (2016).
17. Y. Mukai, H. Hirori, T. Yamamoto, H. Kageyama, and K. Tanaka, "Antiferromagnetic resonance excitation by terahertz magnetic field resonantly enhanced with split ring resonator," Appl. Phys. Lett. **105**, 022410 (2014).
18. M. Sotome, N. Kida, S. Horiuchi, and H. Okamoto, "Visualization of ferroelectric domains in a hydrogen-bonded molecular crystal using emission of terahertz radiation," Appl. Phys. Lett. **105**, 041101 (2014).
19. T. Hofmann, C. Herzinger, C. Krahmer, K. Streubel, and M. Schubert, "The optical Hall effect," Phys. Status Solidi A **205**, 779–783 (2008).
20. N. Karl, M. S. Heimbeck, H. O. Everitt, H.-T. Chen, A. J. Taylor, I. Brener, A. Benz, J. L. Reno, R. Mendis, and D. M. Mittleman, "Characterization of an active metasurface using terahertz ellipsometry," Appl. Phys. Lett. **111**, 191101 (2017).
21. D. Abbott, "Directions in terahertz technology," in *GaAs IC Symposium IEEE Gallium Arsenide Integrated Circuits Symposium*, 22nd annual technical digest (IEEE, 2000), pp. 263–266.
22. J. Chamberlain, "Where optics meets electronics: recent progress in decreasing the terahertz gap," Philos. Trans. R. Soc. London Ser. A **362**, 199–213 (2004).
23. C. Koral, G. Papari, and A. Andreone, "THz spectroscopy of advanced materials," in *Terahertz (THz), Mid Infrared (MIR) and Near Infrared (NIR) Technologies for Protection of Critical Infrastructures Against Explosives and CBRN* (2021), pp. 253–273.
24. G. P. Williams, "Filling the THz gap—high power sources and applications," Rep. Prog. Phys. **69**, 301 (2005).
25. J. S. Melinger, S. S. Harsha, N. Laman, and D. Grischkowsky, "Guided-wave terahertz spectroscopy of molecular solids," J. Opt. Soc. Am. B **26**, A79–A89 (2009).

26. E. Castro-Camus, M. Koch, and A. I. Hernandez-Serrano, “Additive manufacture of photonic components for the terahertz band,” J. Appl. Phys. **127**, 210901 (2020).
27. N. M. Burford and M. O. El-Shenawee, “Review of terahertz photoconductive antenna technology,” Opt. Eng. **56**, 010901 (2017).
28. C. Koral, Z. Mazaheri, G. P. Papari, A. Andreone, I. Drebot, D. Giove, M. R. Masullo, G. Mettivier, M. Opromolla, D. Paparo, A. Passarelli, V. Petrillo, B. Piccirillo, A. Rubano, M. Ruijter, P. Russo, and L. Serafini, “Multi-pass free electron laser assisted spectral and imaging applications in the terahertz/far-IR range using the future superconducting electron source BriXSinO,” Front. Phys. **10**, 725901 (2022).
29. W. Withayachumnankul and M. Naftaly, “Fundamentals of measurement in terahertz time-domain spectroscopy,” J. Infrared, Millim., Terahertz Waves **35**, 610–637 (2014).
30. G. Papari, V. Gargiulo, M. Alfe’, R. Di Capua, A. Pezzella, and A. Andreone, “THz spectroscopy on graphene-like materials for bio-compatible devices,” J. Appl. Phys. **121**, 145107 (2017).
31. A. Pashkin, M. Kempa, H. Nemec, F. Kadlec, and P. Kuzel, “Phase-sensitive time-domain terahertz reflection spectroscopy,” Rev. Sci. Instrum. **74**, 4711–4717 (2003).
32. M. Born and E. Wolf, *Principles of Optics: Electromagnetic Theory of Propagation, Interference and Diffraction of Light* (Elsevier, 2013).
33. X. Chen, E. P. Parrott, B. S.-Y. Ung, and E. Pickwell-MacPherson, “A robust baseline and reference modification and acquisition algorithm for accurate THz imaging,” IEEE Trans. Terahertz Sci. Technol. **7**, 493–501 (2017).
34. S. Fan, E. P. Parrott, B. S. Ung, and E. Pickwell-MacPherson, “Calibration method to improve the accuracy of THz imaging and spectroscopy in reflection geometry,” Photon. Res. **4**, A29–A35 (2016).
35. T. Hofmann, C. Herzinger, A. Boosalis, T. Tiwald, J. A. Woollam, and M. Schubert, “Variable-wavelength frequency-domain terahertz ellipsometry,” Rev. Sci. Instrum. **81**, 023101 (2010).
36. H. Tompkins and E. A. Irene, *Handbook of Ellipsometry* (William Andrew, 2005).
37. P. Kühne, N. Armakavicius, V. Stanishev, C. M. Herzinger, M. Schubert, and V. Darakchieva, “Advanced terahertz frequency-domain ellipsometry instrumentation for in situ and ex situ applications,” IEEE Trans. Terahertz Sci. Technol. **8**, 257–270 (2018).
38. A. A. Galuza, V. K. Kiseliov, I. V. Kolenov, A. I. Belyaeva, and Y. M. Kuleshov, “Developments in THz-range ellipsometry: quasi-optical ellipsometer,” IEEE Trans. Terahertz Sci. Technol. **6**, 183–190 (2016).
39. A. Belyaeva, A. Galuza, I. Kolenov, and S. Mizrakhy, “Developments in terahertz ellipsometry: portable spectroscopic quasi-optical ellipsometer-reflectometer and its applications,” J. Infrared, Millim., Terahertz Waves **42**, 130–153 (2021).
40. I. Azarov, V. Shvets, V. Y. Prokopiev, S. Dulin, S. Rykhlitskii, Y. Choporova, B. Knyazev, V. Kruchinin, and M. Kruchinina, “A terahertz ellipsometer,” Instrum. Exp. Tech. **58**, 381–388 (2015).
41. M. Neshat and N. Armitage, “Terahertz time-domain spectroscopic ellipsometry: instrumentation and calibration,” Opt. Express **20**, 29063–29075 (2012).
42. B. Johs, “Regression calibration method for rotating element ellipsometers,” Thin Solid Films **234**, 395–398 (1993).
43. M. Yamashita, H. Takahashi, and C. Otani, “Ultra-broadband THz time-domain spectroscopic ellipsometry,” Appl. Phys. Lett. **104**, 051103 (2014).
44. X. Chen, E. P. Parrott, Z. Huang, H.-P. Chan, and E. Pickwell-MacPherson, “Robust and accurate terahertz time-domain spectroscopic ellipsometry,” Photon. Res. **6**, 768–775 (2018).
45. M. A. Báez-Chorro and B. Vidal, “Single trace terahertz spectroscopic ellipsometry,” Opt. Express **27**, 35468–35474 (2019).
46. Q. Guo, Y. Zhang, Z. Lyu, D. Zhang, Y. Huang, C. Meng, Z. Zhao, and J. Yuan, “Thz time-domain spectroscopic ellipsometry with simultaneous measurements of orthogonal polarizations,” IEEE Trans. Terahertz Sci. Technol. **9**, 422–429 (2019).
47. V. C. Agulto, T. Iwamoto, H. Kitahara, K. Toya, V. K. Mag-Usara, M. Imanishi, Y. Mori, M. Yoshimura, and M. Nakajima, “Terahertz time-domain ellipsometry with high precision for the evaluation of GaN crystals with carrier densities up to 10^{20} cm^{-3},” Sci. Rep. **11**, 18129 (2021).
48. P. Marsik, K. Sen, J. Khmaladze, M. Yazdi-Rizi, B. P. Mallett, and C. Bernhard, “Terahertz ellipsometry study of the soft mode behavior in ultrathin $SrTiO_3$ films,” Appl. Phys. Lett. **108**, 052901 (2016).
49. M. Neshat and N. Armitage, “Developments in THz range ellipsometry,” J. Infrared, Millim., Terahertz Waves **34**, 682–708 (2013).
50. Z. Mazaheri, C. Koral, and A. Andreone, “Accurate THz ellipsometry using calibration in time domain,” Sci. Rep. **12**, 7342 (2022).
51. M. S. Heimbeck, J. C. Booth, and C. Silver, “Terahertz (THz) optical parameters of three-dimensional (3-D) printing materials,” Tech. rep. (AMRDEC Redstone Arsenal United States, 2017).
52. K. Morino, S. Arakawa, T. Fujii, S. Mouri, T. Araki, and Y. Nanishi, “Characterization of the electrical properties of an InN epilayer using terahertz time-domain spectroscopic ellipsometry,” Jpn. J. Appl. Phys. **58**, SCCB22 (2019).
53. M. Ney and I. Abdulhalim, II, “Modeling of reflectometric and ellipsometric spectra from the skin in the terahertz and submillimeter waves region,” J. Biomed. Opt. **16**, 067006 (2011).
54. D. Grischkowsky, S. Keiding, M. Van Exter, and C. Fattinger, “Far-infrared time-domain spectroscopy with terahertz beams of dielectrics and semiconductors,” J. Opt. Soc. Am. B **7**, 2006–2015 (1990).
55. M. Naftaly and A. Gregory, “Terahertz and microwave optical properties of single-crystal quartz and vitreous silica and the behavior of the boson peak,” Appl. Sci. **11**, 6733 (2021).
56. J. F. O’Hara, W. Withayachumnankul, and I. Al-Naib, “A review on thin-film sensing with terahertz waves,” J. Infrared, Millim., Terahertz Waves **33**, 245–291 (2012).
57. J. Tang, L. Y. Deng, C. B. Tay, X. H. Zhang, J. W. Chai, H. Qin, H. W. Liu, T. Venkatesan, and S. J. Chua, “Determination of carrier concentration dependent electron effective mass and scattering time of n-ZnO thin film by terahertz time domain spectroscopy,” J. Appl. Phys. **115**, 033111 (2014).
58. C.-W. Chen, Y.-C. Lin, C.-H. Chang, P. Yu, J.-M. Shieh, and C.-L. Pan, “Frequency-dependent complex conductivities and dielectric responses of indium tin oxide thin films from the visible to the far-infrared,” IEEE J. Quantum Electron. **46**, 1746–1754 (2010).

93.146.169.131 {ts '2022-12-08 08:04:24'}